







Article

Electrochemical Noise Analysis in Passivated Martensitic Precipitation-Hardening Stainless Steels in H₂SO₄ and NaCl Solutions

Facundo Almeraya-Calderon ¹, Miguel Villegas-Tovar ¹, Erick Maldonado-Bandala ², Demetrio Nieves-Mendoza ², Ce Tochtli Méndez-Ramírez ^{2,*}, Miguel Angel Baltazar-Zamora ², Javier Olguín-Coca ³, Luis Daimir Lopez-Leon ³, Griselda Santiago-Hurtado ⁴, Verónica Almaguer-Cantu ⁵, Jesus Manuel Jaquez-Muñoz ⁶ and Citlalli Gaona-Tiburcio ^{1,*}

- ¹ Universidad Autónoma de Nuevo León, FIME, Centro de Investigación e Innovación en Ingeniería Aeronáutica (CIIA), San Nicolás de los Garza 66455, Mexico; facundo.almerayacl@uanl.edu.mx (F.A.-C.); miguel.villegastvr@uanl.edu.mx (M.V.-T.)
 - ² Facultad de Ingeniería Civil, Universidad Veracruzana, Xalapa 91000, Mexico; erimaldonado@uv.mx (E.M.-B.); dnieves@uv.mx (D.N.-M.); mbaltazar@uv.mx (M.A.B.-Z.)
 - ³ Área Académica de Ingeniería y Arquitectura, Universidad Autónoma del Estado de Hidalgo, Carretera Pachuca-Tulancingo Km. 4.5., Pachuca 42082, Mexico; olguinc@uaeh.edu.mx (J.O.-C.); luis_lopez@uaeh.edu.mx (L.D.L.-L.)
 - ⁴ Facultad de Ingeniería Civil, Universidad Autónoma de Coahuila, Torreón 27276, Mexico; santiagoog@uadec.edu.mx
 - ⁵ Instituto de Biotecnología, Facultad de Ciencias Biológicas, Universidad Autónoma de Nuevo León, San Nicolás de los Garza 66455, Mexico; veronica.almaguerct@uanl.edu.mx
 - ⁶ Centro de Ciencias de la Ingeniería, Universidad Autónoma de Aguascalientes, Aguascalientes 20340, Mexico; jesus.jm01@cdjuarez.tecnm.mx
- * Correspondence: cmendez@uv.mx (C.T.M.-R.); citlalli.gaonatbr@uanl.edu.mx (C.G.-T.)



Academic Editors: Fei Yin, Lin Hua, Jian Wang, Nong Gao and Petros E. Tsakiridis

Received: 19 June 2025

Revised: 19 July 2025

Accepted: 24 July 2025

Published: 26 July 2025

Citation: Almeraya-Calderon, F.; Villegas-Tovar, M.; Maldonado-Bandala, E.; Nieves-Mendoza, D.; Méndez-Ramírez, C.T.; Baltazar-Zamora, M.A.; Olguín-Coca, J.; Lopez-Leon, L.D.; Santiago-Hurtado, G.; Almaguer-Cantu, V.; et al.

Electrochemical Noise Analysis in Passivated Martensitic Precipitation-Hardening Stainless Steels in H₂SO₄ and NaCl Solutions. *Metals* **2025**, *15*, 837. <https://doi.org/10.3390/met15080837>

Copyright: © 2025 by the authors. Licensee MDPI, Basel, Switzerland. This article is an open access article distributed under the terms and conditions of the Creative Commons Attribution (CC BY) license (<https://creativecommons.org/licenses/by/4.0/>).

Abstract

Precipitation-hardenable stainless steels (PHSS) are widely used in various applications in the aeronautical industry such as landing gear supports, actuators, and fasteners, among others. This research aims to study the pitting corrosion behavior of passivated martensitic precipitation-hardening stainless steel, which underwent passivation for 120 min at 25 °C and 50 °C in citric and nitric acid baths before being immersed in solutions containing 1 wt.% sulfuric acid (H₂SO₄) and 5 wt.% sodium chloride (NaCl). Electrochemical characterization was realized employing electrochemical noise (EN), while microstructural analysis employed scanning electron microscopy (SEM). The result indicates that EN reflects localized pitting corrosion mechanisms. Samples exposed to H₂SO₄ revealed activation–passivation behavior, whereas those immersed in NaCl exhibited pseudo-passivation, indicative of an unstable oxide film. Current densities in both solutions ranged from 10^{−3} to 10^{−5} mA/cm², confirming susceptibility to localized pitting corrosion in all test conditions. The susceptibility to localized attack is associated with the generation of secondary oxides on the surface.

Keywords: corrosion; passivation; martensitic stainless steel; electrochemical noise

1. Introduction

In the aerospace industry, a variety of components such as actuators, landing gear supports, and fasteners are manufactured from stainless steel because these materials offer good mechanical strength and corrosion resistance in the presence of aggressive

atmospheres. In different industry sectors, corrosion causes significant economic losses. In the aeronautical industry, costs vary and are associated with various factors such as industry regulations, preventive maintenance practices, and technological advances [1–4].

Stainless steels are alloys containing [Fe-Cr] (at least 11% chromium) with nickel additions and have a variety of applications. Stainless steels can be classified based on their microstructure and precipitates, as ferritic, austenitic, martensitic, duplex, and precipitation hardening (PH) [5,6]. The aeronautical industry relies on precipitation-hardenable (PH) steels for their superior properties, including low weight, high mechanical strength, and excellent corrosion resistance. PH stainless steels (PHSS) fall into two categories: semi-austenitic, known for high ductility and corrosion resistance, and martensitic, valued for their strength-to-weight ratio [7–11]. Key industrial stainless steels like 17-4PH, 17-7PH, and 15-7Mo were introduced by Armco (USA) in 1948, followed by semi-austenitic AM350 and AM355, and martensitic Custom 630, 455, and 450, produced by Carpenter Technology Corporation and ATI Materials. These steels serve in turbine blade, rotor, and shaft manufacturing. Additionally, 15-5 PH steel from Penn Stainless Products, Inc., is used in aircraft structural components [12–14].

Alloys such as stainless steels have high corrosion resistance performance due to the protective film of chromium oxide (Cr_2O_3) that forms on the surface and is characterized by being a thin, invisible, and compact film. The chemical treatment that allows the growth of the oxidation film is known as passivation and improves corrosion resistance. Passivation treatment was discovered by chemist Christian Friedrich Schönbein in the mid-19th century, and is commonly performed on stainless steels using an oxidizing agent such as nitric acid [15–21]. The addition of elements such as Cr with Mo decreases pitting corrosion. Also, elements such as N and Cu can help reduce these problems. The passive film of Cr plays a crucial role in reducing the corrosion rate; however, SS has transitioned from a single passivation trend to exhibiting pitting corrosion [22,23]. Surface factors (heterogeneity, roughness, microstructure, etc.) are important to determine the corrosion behavior of material; defects in the atomic layer, the difference in phases, and roughness will reduce the corrosion resistance [24–26]. Factors such as reducing gases, alkaline solutions, mechanical wear, or non-oxidizing acids can disrupt the oxide film, accumulating corrosion products in specific zones [27,28].

Different studies [29–32] propose that citric acid could serve as an environmentally friendly alternative to nitric acid, which is widely used for anti-corrosion treatments. Adjusting specific parameters, such as duration, temperature, and electrolytic baths during passivation has enhanced the passive layer's properties. It is also crucial to recognize that anodic reactions involving iron dissolution lead to chromium and iron oxide films forming, which create the passive layer characteristic of stainless steel, ensuring corrosion resistance [33].

Research on the corrosion behavior of stainless steels has focused on accelerated corrosion testing (salt spray chamber) and localized corrosion, pitting nucleation, and passive, pseudopassive, and transpassive zones to understand the corrosion mechanisms of these steels. Corrosion studies have been conducted using electrochemical techniques such as potentiodynamic (PP) and galvanodynamic (PG) polarization, cyclic potentiodynamic polarization (CPP), electrochemical impedance spectroscopy (EIS), and electrochemical noise (EN). The latter technique has allowed for data analysis in time, time-frequency, and frequency, respectively [14–21]. However, the literature on the corrosion of PH steels is limited, and it is necessary to determine the corrosion mechanism and the behavior of the passive layer that forms.

Some of the stainless steel passivation studies using electrochemical techniques are summarized as follows: the electrochemical noise technique used by Suresh and Mudali

in 2014 [34] analyzed the corrosion behavior of austenitic 304 stainless steel immersed in ferric chloride (FeCl_3), finding an important relationship between the frequency analysis through power spectral density (PSD) and time analysis (statistical study, noise resistance (R_n) and localization index (IL)) to find the localized pitting corrosion mechanism. In 2018, Lara et al. [35], investigated precipitation-hardenable steels, having as reference an austenitic 304 steel; the corrosion kinetics were studied by electrochemical noise in the current and potential mode, potentiodynamic polarization tests were reported, and the passivation process was carried out using citric acid as an environmentally friendly option; the results indicated that the passivation films formed were different in the different passivation acids, as the evaluations were carried out in sulfuric acid and sodium chloride. In other investigations, potentiodynamic polarization and electrochemical impedance spectroscopy were used to study the oxide film through charge transfer processes in authentic passivated stainless steels such as 304 [36]. The electrochemical characteristics of SS have also been studied by varying the pH concentrations in aerated solutions, resulting in a decrease in the pH of the oxidizing solution that promotes the formation of protective films, improving the corrosion resistance of the substrates [37–41]. Pei-de Han et al., in 2022–2023, studied superaustenitic steel S31254 by potentiodynamic polarization and electrochemical impedance spectroscopy to see the effect of boron on the dissolution and repair of the passive films of these steels, in the presence of sulfuric acid; they resulted in better corrosion resistance with the addition of boron [42,43].

Recent investigations on PHSS, such as CUSTOM450 (martensitic) and AM350 (austenitic) steels, have focused on hydrogen diffusion, fatigue behavior, and microstructural characterization [44–47]. Samaniego et al. [4,8,20] studied the corrosion behavior of CUSTOM450- and AM350-passivated PHSS steels using electrochemical noise and electrochemical impedance spectroscopy in acid baths. The CUSTOM 450 PHSS showed the best results in corrosion behavior in acid baths. The primary research for this type of alloy has been conducted using potentiodynamic polarization and spectroscopy impedance. Therefore, this research will utilize EN to investigate the transient behavior and its correlation with corrosion.

This study analyzed the pitting corrosion of martensitic precipitation-hardening stainless steel that had been passivated for 120 min at 25 and 50 °C using citric and nitric acid baths and then immersed in solutions containing 1 wt.% sulfuric acid and 5 wt.% sodium chloride. The electrochemical technique was electrochemical noise based on ASTM G199-90. [48,49] The EN technique was analyzed, employing methods of classic statistics and recurrence plots (RP). The RP is used for chaotic signals, as are the corrosion signals. Few researchers used that method to study. The microstructural analysis was performed by scanning electron microscopy (SEM) after the samples had been tested for corrosion. Corrosion studies on stainless steels in recent years have focused on austenitic steels. PHSS steels have few studies; these steels are used in components that require a combination of excellent mechanical properties, as well as corrosion resistance due to aircraft exposure in harsh environments. So, it is important to know the electrochemical corrosion in electrolytes where aircraft commonly work, so that they can simulate marine, industrial (acid rain), and urban atmospheres.

2. Materials and Methods

2.1. Materials

The commercial martensitic precipitation-hardening stainless steel used is equivalent to CUSTOM 450 (AMS 5773, AMS Aerospace Material Specifications) in the shape of rolled and heat-treated cylindrical bars. Stainless steel was employed and tested in the

as-received condition; the nominal chemical composition of these stainless steels is shown in Table 1 [50].

Table 1. Chemical composition of the martensitic PHSS (wt.%).

Element	Martensitic PHSS
Cr	14.0–16.0
Ni	5.0–7.0
Mo	0.50–1.0
Mn	1.00 max
Cu	1.25–1.75
Nb	0.35–0.75
N	≤0.1
Si	1.00 max
S	0.030
C	≤0.05
Fe	Balance

The metallography technique was used to prepared martensitic stainless steel samples using silicon carbide sandpaper of varying grades (240, 400, 500, 600, and 800). For corrosion tests the surface samples were roughened and polished using diamond paste, and then cleaned with deionized water and ultrasound in ethanol for 10 min [51,52]. The microstructure of martensitic PHSS was assessed using optical microscopy (OM, Olympus, Hamburg, Germany). Using the metallography technique (roughing was performed from 240 to 4000 grit, and the polishing of the samples with a diamond paste), to reveal the microstructure with a chemical agent called Fry's, which was composed of 5 g CuCl, 40 mL HCl, 30 mL H₂O, and 25 mL of ethanol.

2.2. Microstructure of Martensitic PHSS

Figure 1 displays the microstructure of martensitic precipitation-hardening stainless steel using optical microscopy. It shows the martensitic phase (α') and remnants of retained austenite (γ), respectively.

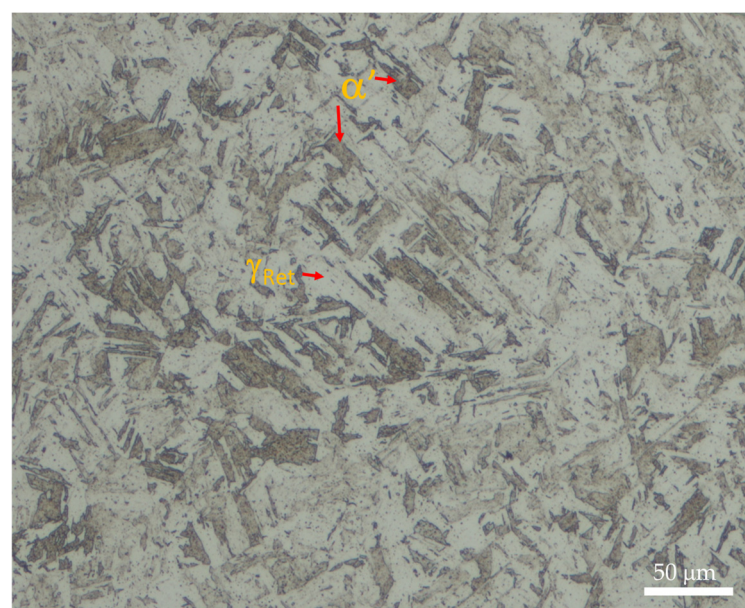


Figure 1. Martensitic PHSS microstructure analyzed by optical microscopy (Initial conditions), 200 \times .

Martensitic precipitation-hardening stainless steel offers moderate mechanical strength and outstanding corrosion resistance. When annealed, it achieves a yield strength exceeding 100 ksi (689 MPa); but through a single-stage heat hardening process it further enhances toughness, ductility, and mechanical strength. The chosen aging temperature affects the mechanical characteristics [52].

2.3. Chemical Passivation Treatment

The chemical passivation treatment on stainless steel was carried out based on the ASTM A967-17 standard [15]. The procedure was carried out based on the stages mentioned in the following experimental diagram (Figure 2) [53–55]:

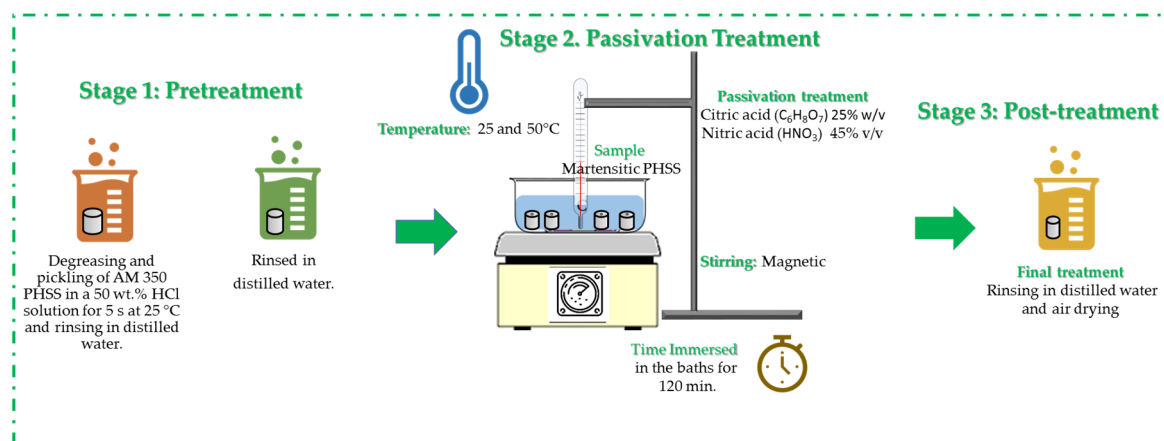


Figure 2. Diagram of the stages of passivation treatment.

To identify each of the samples, the nomenclature in Table 2 was used (time and material are omitted as they are constant parameters): The electrolytes are identified as 1 for H₂SO₄ and 2 for NaCl, the passivation baths C for citric acid and N for nitric acid, and the temperature values are 25 and 50 °C, respectively. The description of all the parameters of each of the samples tested is indicated in Table 2.

Table 2. General characteristics of the martensitic precipitation-hardening stainless steel samples.

Electrolyte	Temperature (°C)	Time (min)	Passivation Baths	Nomenclature
H ₂ SO ₄ (1)	25	120	Citric Acid C ₆ H ₈ O ₇ (25% w/v)	1/C/25
	50			1/C/50
	25	120	Nitric Acid HNO ₃ (45% v/v)	1/N/25
	50			1/N/50
NaCl (2)	25	120	Citric Acid C ₆ H ₈ O ₇ (25% w/v)	2/C/25
	50			2/C/50
	25	120	Nitric Acid HNO ₃ (45% v/v)	2/N/25
	50			2/N/50

2.4. Corrosion Measurement

Electrochemical corrosion measurements were performed to determine martensitic precipitation-hardening stainless steel pitting corrosion using the electrochemical technique of electrochemical noise. Martensitic PHSS samples had an area of 1.0 cm² and

were immersed in two solutions: 1 wt% sulfuric acid and 5 wt% sodium chloride at room temperature (25 ± 2 °C) [4,8,14]. For each experiment, two nominally identical specimens were used as the working electrodes (WE1 and WE2) and a saturated calomel electrode as the reference electrode (RE). Electrochemical current noise (ECN) was measured with a galvanic coupling current between two identical working electrodes; simultaneously, electrochemical potential noise (EPN) was measured linking one of the working electrodes and a reference electrode. The electrochemical equipment was a potentiostat/galvanostat/ZRA (produced by Solartron 1287A, Bognor Regis, UK). Electrochemical corrosion tests were performed in triplicate.

Electrochemical noise measurements were based on ASTM G199-09 [56], acquiring 1024 data points at 1 data/second speed. A program created with MATLAB 2018a software from Math Works (Natick, MA, USA) was used to process the EN data [56–58].

2.5. Microstructural Characterization

The surface analysis after corrosion testing was conducted with a scanning electron microscope (SEM, JEOL-JSM-5610LV, Tokyo, Japan) equipped with a secondary electron (SE) detector. The SEM operated at a beam energy of 20 kV and a working distance of 11–13 mm.

3. Results and Discussion

3.1. Corrosion Measurements

Electrochemical Noise

Electrochemical noise (EN) refers to spontaneous, low-level fluctuations in potential and current during electrochemical processes. This technique is particularly effective for monitoring localized corrosion, as its analysis depends on the signal type within the system. A major advantage of EN is its ability to assess localized corrosion through a non-invasive approach [59–62].

EN analysis is divided into time-domain, frequency-domain, frequency-time, and chaotic systems. Initially, signals underwent statistical evaluation, with researchers such as Mansfeld, Cottis, Turgosse, Eden, and Bertocci investigating the correlation between corrosion types and statistical metrics like localization index (LI) and pitting index, derived from standard deviations of ECN and EPN. Additionally, the noise resistance (R_n) parameter was introduced as an R_p equivalent, linking it to kinetic properties. Later studies incorporated kurtosis and skewness to refine LI for improved corrosion classification [63–70].

EN signals comprise DC, stationary, and random components. Separating DC from the stationary and random components is essential to analyze EN data effectively, as DC can distort statistical, visual, and power spectral density (PSD) evaluations by introducing artificial frequencies. Once DC is removed, low-frequency corrosion data remain unaffected. EN can be mathematically represented, as shown in Equation (1), where $x(t)$ is the EN time series, m_t is the DC component, s_t is the random component, and Y_t is a stationary component. The last two are functions that define the corrosion system [71–76]:

$$x(t) = m_t + s_t + Y_t \quad (1)$$

To calculate noise resistance (R_n), the standard deviation from time series data must be determined. These statistical parameters offer insights into corrosion mechanisms and kinetics. Research by Turgoose and Cottis [63] revealed that higher corrosion rates correspond to variance and standard deviation increases. Use Equation (2) to compute the standard deviation (σ), standard deviation of the potential data (σ_v), standard deviation of

the potential data (σ_I), working electrode area (A), and derive R_n (Equation (3)), utilizing EN time series information (EPN and ECN) as the foundation:

$$\sigma_x = \sqrt{x^2} = \sqrt{\frac{\sum_{i=1}^N (x_i - \bar{x})^2}{N}} \quad (2)$$

$$R_n = \frac{\sigma_v}{\sigma_I} \times A \quad (3)$$

This study employed kurtosis and skewness to classify corrosion types. However, the localization index (LI) was excluded, as Mansfeld and Sun [71] concluded in 1995 that it has limitations and requires cautious application. A patent created by Reid and Eden in 2001 [77] proposed that statistical moments, including skewness and kurtosis, can be utilized to determine the corrosion type. These correspond to the third and fourth statistical moments [77,78]. The following table shows the relationship between the values obtained by kurtosis and skewness to determine the corrosion type of material (Table 3).

Table 3. Corrosion types are evaluated by kurtosis and skewness.

Corrosion Type	Potential Skewness	Kurtosis	Current Skewness	Kurtosis
Uniform	$<\pm 1$	<3	$<\pm 1$	<3
Pitting	<-2	$>>3$	$>\pm 2$	$>>3$
Transgranular (SCC)	4	20	-4	20
Intergranular (SCC #1)	-6.6	18 to 114	1.5 to 3.2	6.4 to 15.6
Intergranular (SCC #2)	-2 to -6	5 to 45	3 to 6	10 to 60

Figure 3 shows the time series of passivated martensitic precipitation-hardening stainless steel exposed to H_2SO_4 . Figure 3a shows how the sample 1/N/50 presented higher amplitudes with values of 4×10^{-4} V, but the potential begins to be reduced. All the signals presented a high transitory number. Figure 3b shows the time in the current series; it presents a high transitory number with an amplitude higher for samples 1/C/50 and 1/N/50. The high number of transmissions indicates much pitting on the material surface. That behavior is reflected in Table 4, where the LI of samples 1/C/50 and 1/N/50 are associated with localized corrosion.

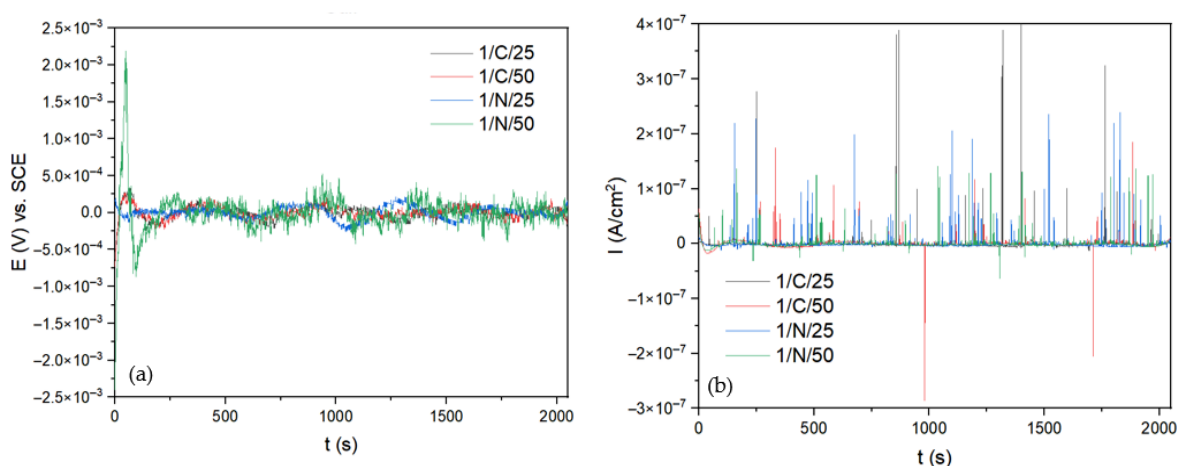


Figure 3. Time series of electrochemical noise (a) potential and (b) current of martensitic precipitation-hardening stainless steel exposed to H_2SO_4 solution.

Table 4. Parameters obtained by EN for martensitic precipitation-hardening stainless steel in 1 wt.% H₂SO₄ and 5 wt% NaCl solutions.

Electrolyte	Parameters	Samples			
		1/C/25	1/C/50	1/N/25	1/N/50
H ₂ SO ₄	R _n (Ω·cm ²)	4060 ± 9	7027 ± 5	4734 ± 4	22146 ± 6
	LI	0.07 ± 0.002	0.1 ± 0.002	0.2 ± 0.002	0.4 ± 0.002
	Kurtosis	258 ± 3	240 ± 2	116 ± 2	83 ± 2
	Skewness	15 ± 2.1	−3.7 ± 0.5	9.9 ± 0.6	8.1 ± 0.2
NaCl	R _n (Ω·cm ²)	716 ± 7	1716 ± 11	2102 ± 13	44985 ± 16
	LI	0.06 ± 0.002	0.02 ± 0.001	0.1 ± 0.001	0.06 ± 0.001
	Kurtosis	12 ± 0.01	13 ± 0.004	8 ± 0.005	49 ± 0.006
	Skewness	−1.5 ± 0.04	1.1 ± 0.01	−1.5 ± 0.05	3.2 ± 0.04

On the other hand, 1/C/25 presented a mixed corrosion process with a value of 0.07, indicating that both processes are occurring on the surface. In the kurtosis and skewness evaluation, all samples presented values related to pitting corrosion. The sample 1/N/50 exhibited a higher R_n value (22146 Ω·cm²). Additionally, the sample passivated at 50 °C in citric acid showed the second-highest R_n value of 7027 Ω·cm², indicating that when passivation temperature increases, the corrosion resistance of passivated steel increases. The samples specified at 25 °C presented 4000 Ω·cm² values with less corrosion resistance.

Figure 4 shows the time series of martensitic precipitation-hardening stainless steel exposed to NaCl. Figure 4a shows the potential time series, where 1/25/N presents a high amplitude with values of 14×10^{-2} V at the beginning but with a decrease in amplitude; that behavior is presented by the rest of the samples, indicating that a reduction of ionic transference occurs due to a stabilization of the material's surface. The current in time series (Figure 4b) shows that sample 1/N/50 presented a lower amplitude than the other samples; that behavior is associated with a lower corrosion kinetic, so 1/N/50 presented the highest R_n with 44,965 Ω·cm². In this medium, the samples passivated in citric acid presented the lower corrosion rate resistance with 700 and 1700 Ω·cm², respectively. However, the samples exposed to citric acid LI values related to the mixed corrosion process and 1/N/50. All the kurtosis results indicated to localized corrosion occurs; however, skewness shows how 1/C/50 has a value of uniform corrosion. The rest of the values are related to localized corrosion; however, the values are very close to the division of localized to uniform corrosion.

Non-linear (chaotic) systems can be analyzed using recurrence plots (RPs), which identify whether processes follow deterministic recurrence patterns. If a system is deterministic (D), it corresponds to localized processes, whereas recurrence in its domain suggests uniform behavior [61,62].

A recurrence plot (RP) is a two-dimensional binary diagram illustrating temporal patterns in a single observable time series, such as current (I) in this study. It represents trajectory recurrences (xi in Rm) at specific time points (i, j) within an (m)-dimensional phase space and a defined threshold (ε). The RP consists of a square matrix with black and white dots along time axes (ti, tj), where black dots mark state recurrences at position (ti, tj); The matrix formulation is provided in Equation (4) [78,79]:

$$R_{ij} = \Theta\left(\varepsilon - \left\|\vec{x}_i - \vec{x}_j\right\|\right), i, j = 1, \dots, N \quad (4)$$

Figure 5 shows the recurrence plots of samples exposed to H_2SO_4 . Figure 5a shows the behavior of 1/C/25. This sample exhibited a localized process trend, similar to Figure 5b, where the samples were transitory. However, the number of vertical and horizontal lines indicate that the localized process occurs periodically; therefore, for that reason, the determinism value (DET) from Table 5, of all the samples, is between 0.93 and 0.87, and the recurrence (RR) with values are from 0.2 to 0.60. Also, trapping time (TT), the value associated with the repeatability time, is between 6 and 12, indicating that the process is repeated too periodically. That suggests that a pitting uniform corrosion process is probably occurring on the surface. Also, the breaking and passivation of a passive layer is associated with this behavior.

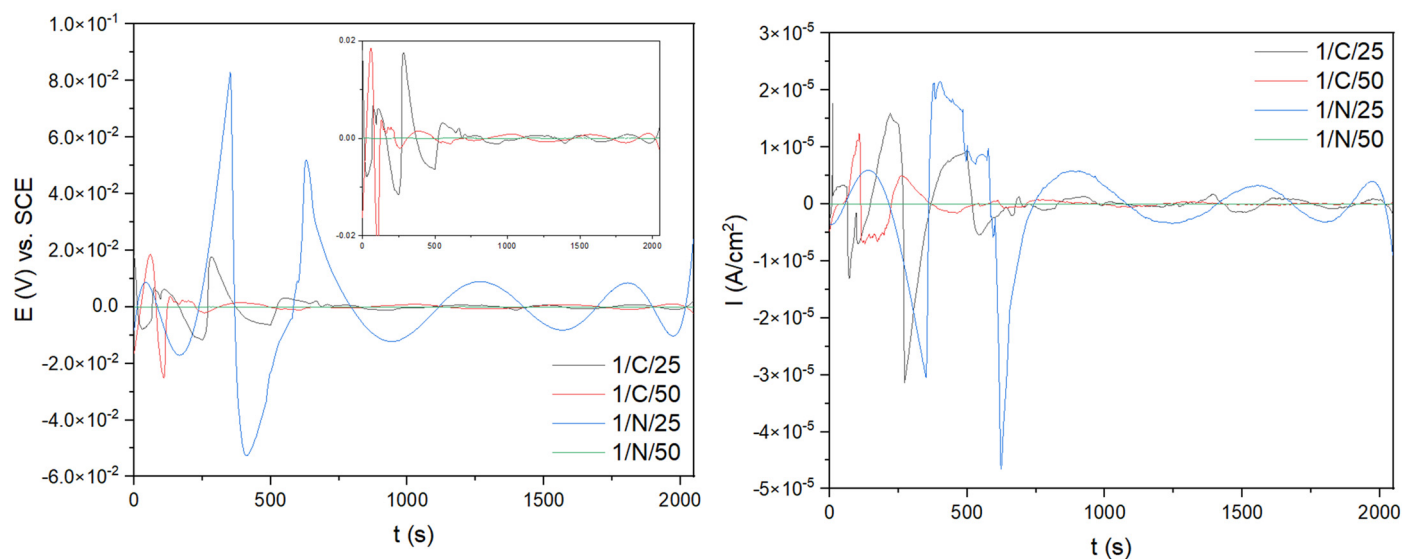


Figure 4. Time series of electrochemical noise (a) potential and (b) current of martensitic precipitation-hardening stainless steel exposed to NaCl solution.

Table 5. Parameters obtained by recurrence plot analysis for martensitic precipitation-hardening stainless steel in 1 wt.% H_2SO_4 and 5 wt% NaCl solutions.

Electrolyte	Parameters	Samples			
		1/C/25	1/C/50	1/N/25	1/N/50
H_2SO_4	RR	0.606 ± 0.006	0.211 ± 0.005	0.5 ± 0.01	0.295 ± 0.006
	Det	0.937 ± 0.003	0.827 ± 0.002	0.871 ± 0.002	0.856 ± 0.008
	L	7.72 ± 0.004	4.682 ± 0.006	4.468 ± 0.005	4.204 ± 0.004
	LAM	0.962 ± 0.005	0.902 ± 0.002	0.932 ± 0.002	0.924 ± 0.005
	TT	12.5 ± 0.01	7.14 ± 0.01	6.85 ± 0.01	6.34 ± 0.01
NaCl	RR	0.196 ± 0.002	0.255 ± 0.001	0.113 ± 0.004	0.096 ± 0.004
	Det	0.992 ± 0.006	0.992 ± 0.008	0.986 ± 0.005	0.386 ± 0.004
	L	20.82 ± 0.05	20.46 ± 0.02	24.61 ± 0.03	2.33 ± 0.02
	LAM	0.996 ± 0.002	0.996 ± 0.001	0.993 ± 0.002	0.493 ± 0.004
	TT	30.905 ± 0.002	32.635 ± 0.002	31.327 ± 0.002	2.576 ± 0.002

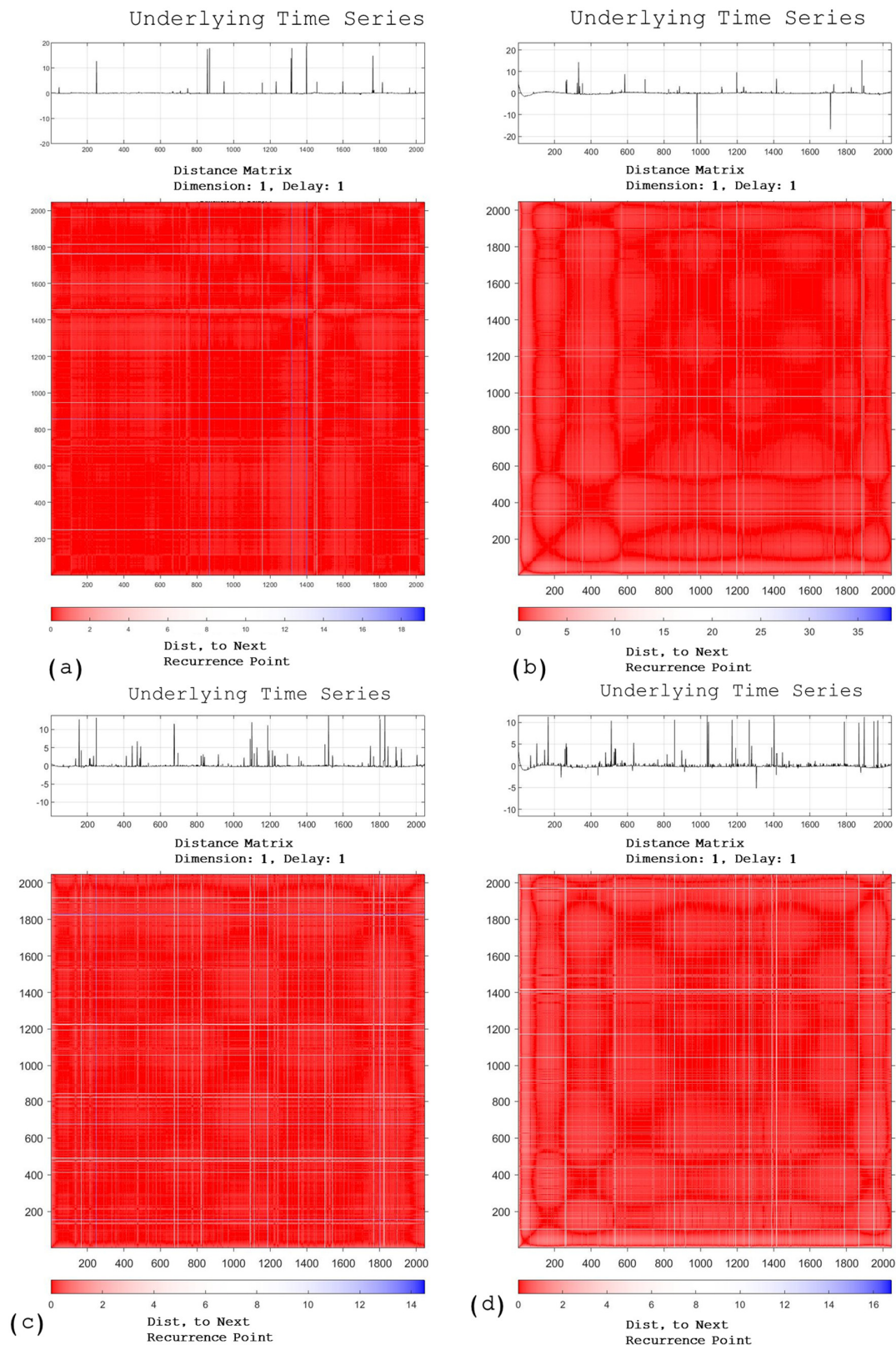


Figure 5. Recurrence plots of martensitic precipitation-hardening stainless steel. (a) 1/C/25, (b) 1/C/50, (c) 1/N/25, and (d) 1/N/50 exposed to H_2SO_4 solution.

Figure 6 shows the recurrence plots of samples exposed to NaCl. The behaviors of samples 1/C/25, 1/C/50, and 1/N/25 are similar, with localized processes before the second 1000 and the lack of transience. This behavior is related to localized corrosion with a low frequency; hence, the TT value is lower. On the other hand, sample 1/N/50 pre-

sented multiple lines vertically and horizontally, with values associated with linearity (L), indicating uniform corrosion on the surface. It can be associated with a passivation process.

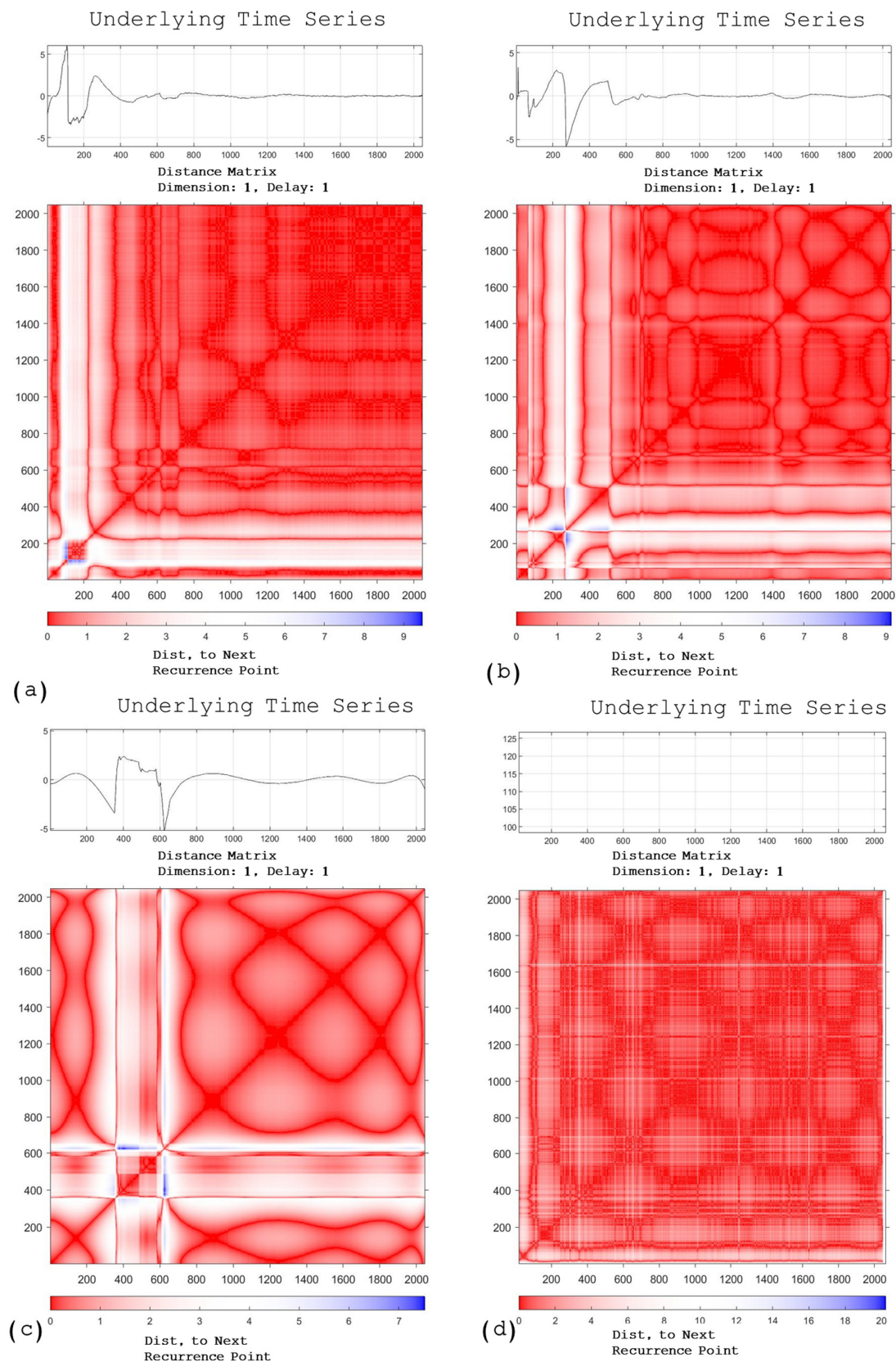


Figure 6. Recurrence plots of martensitic precipitation-hardening stainless steel. (a) 1/C/25, (b) 1/C/50, (c) 1/N/25, and (d) 1/N/50 exposed to NaCl.

3.2. SEM Characterization of PHSS After Electrochemical Corrosion Measurements

Following electrochemical corrosion measurements, the surface morphology of each sample was examined using SEM to study the reaction of materials against corrosion. SEM analysis revealed that localized pitting corrosion occurred on all passivated stainless steel surfaces, with some conditions only showing pit nucleation, while others demonstrated severe localized attack.

The martensitic PHSS passivated at 25 and 50 °C (Figure 7a–d) was exposed to H₂SO₄ and presented pit nucleation with pits measuring approximately 10 microns in size.

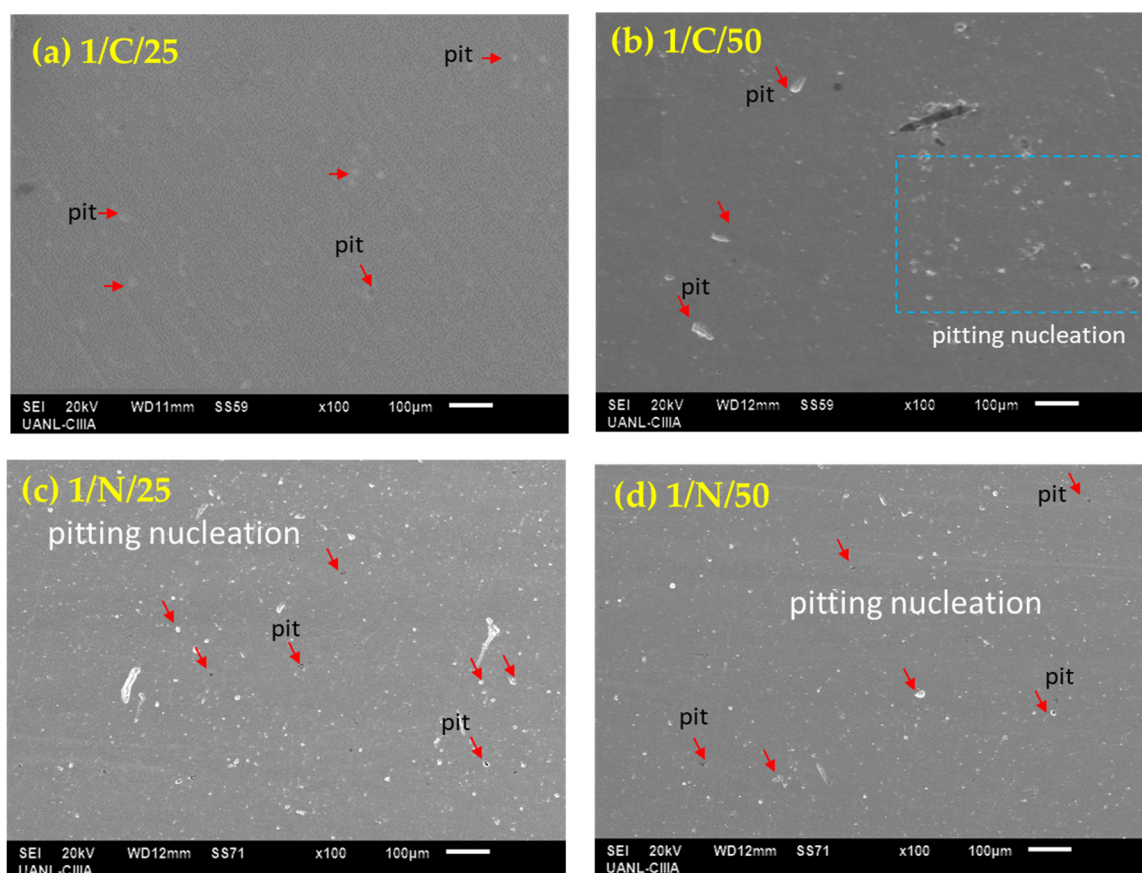


Figure 7. SEM-SE surface morphology of passivated martensitic precipitation-hardening stainless steel in citric (a,b) and nitric (c,d) acids at 25 and 50 °C for 120 min, exposed in H₂SO₄ solutions (after corrosion testing).

For the martensitic precipitation-hardening stainless steel immersed in NaCl under similar passivation conditions (Figure 8a–d), pitting corrosion was observed with pit sizes exceeding 100 microns.

In previous studies, precipitation-hardening martensitic stainless steels displayed distinctive profiles due to different electrochemical behavior in NaCl and H₂SO₄ test solutions, indicating passivation during the anodic reaction, along with variability in pitting potentials. When martensitic stainless steel is immersed in H₂SO₄ solution, a passivation layer forms on the surface of the chromium-rich alloy, improving corrosion resistance and initiating protective mechanisms. Iron and chromium oxides play a critical role in creating the passive film in stainless steels by interacting with hydroxyl ions. High current densities in martensitic stainless-steel samples result in transpassivation and secondary passivation. On the other hand, samples immersed in NaCl solution exhibit pseudo-passivation, reflecting the presence of an unstable protective layer. This defense system

forms a passive Cr-rich oxide and oxyhydroxide film that protects the substrate from chloride ions (Cl^-) while preventing oxygen penetration into the inner layer [30,31,80].

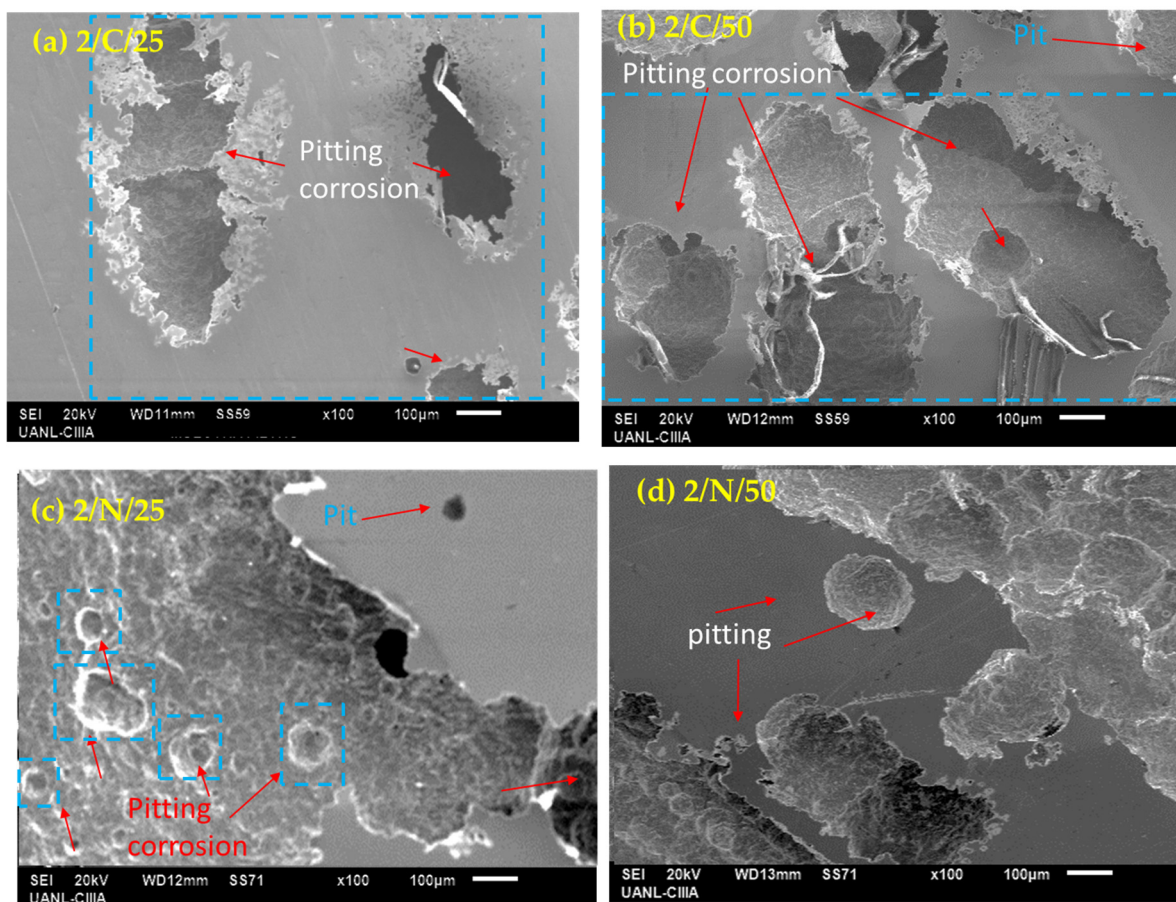
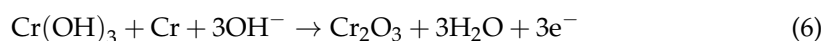
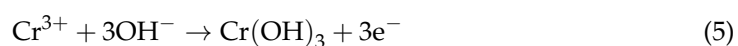


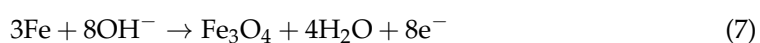
Figure 8. SEM-SE surface morphology of passivated martensitic precipitation-hardening stainless steel in citric (a,b) and nitric (c,d) acids at 25 and 50 °C for 120 min, exposed in NaCl solutions (after corrosion testing).

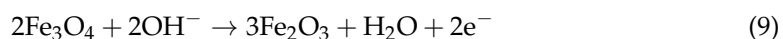
According to various authors [31,32], unstable passivation layers increase current density in stainless steels exposed to NaCl, thus altering corrosion kinetics. In contrast, austenitic stainless steels in H_2SO_4 solutions displayed transient phenomena linked to transpassivation, characterized by passive film disruption, and secondary passivation, associated with passive layer regeneration.

The passive region is the formation site for iron oxide and chromium oxide coatings, often identified in martensitic stainless steel [32,81–84]. The selective dissolution of Cr^{3+} from the stainless-steel surface results in the chromium trihydroxide complex, $\text{Cr}(\text{OH})_3$ (Equation (5)). Subsequently, $\text{Cr}(\text{OH})_3$ reacts to develop a continuous chromium oxide passive layer, Cr_2O_3 , on the surface (Equation (6)) [32,85]:



As mentioned before, iron and chromium oxidation mainly cause anodic reactions during the passivation film development stage. The iron oxidation processes are illustrated in Equations (7)–(9) [32,86,87]:





Passivated martensitic precipitation-hardening stainless steel samples immersed in sulfuric acid under both passivation conditions exhibit pseudo-passivation, characterized by an unstable oxide layer alongside distinct secondary passivation. Research suggests that the $\text{Cr}(\text{OH})_3$ film's formation may be connected to this pseudo-passivation behavior [88,89].

The samples passivated in nitric acid performed better at 50 °C than at 25 °C. The diffusion process of passivation in nitric acid is more straightforward and generates a more stable passive layer due to the exothermic properties of nitric acid. On the other hand, citric acid is an endothermal chemical, and the properties of the oxide layer generated at 50 °C decreased the corrosion resistance [88].

The electrochemical noise results show that samples exposed to H_2SO_4 presented a lower value of TT, indicating that pitting attack occurs recurrently. That behavior means that the pitting attack is uniform. That is, pitting nucleation occurs (as SEM shows). On the other hand, when the sample is exposed to NaCl, it presents a localized attack. That behavior is related to Cl^- ions' preference to attack the sample surface in specific zones, generating the localization of corrosion.

Various researchers have applied recurrence plots (RP) to classify corrosion types [32,61,81–83,90–92]. Valavanis et al. [93] propose that RP is useful for identifying dynamic states, transitions, and complex physicochemical processes such as passivity, pitting, and uniform corrosion. Garcia-Ochoa [92] highlights RP's role in analyzing non-linear systems and electrochemical processes, emphasizing its necessity for scientific disciplines requiring such assessments. Since corrosion behaves as a chaotic or non-linear system [94,95], RP and recurrence quantification analysis (RQA) provide valuable insights into the corrosion process.

EN showed the types of corrosion and the stability of the passive layer; however, some transients were present. It occurs due to the instability of the oxide passive layer created in the sample. This will be dissolved when an oxide soluble in an aqueous solution is generated. However, the presence of multiple alloying elements such as Ni, Mo, Mn, Cu, and hydroxides facilitates the generation of other oxides that can be unstable under aqueous media. As a secondary oxide layer is generated, the corrosion process begins to occur in those specific zones. Figure 9 shows how localized attacks occur on another passive layer. Also, information obtained from SEM-EDS shows how elements such as Ni, Cu, and Fe are present on the surface. Hence, the corrosive ions attack the more susceptible oxides (solubility, porosity, and/or cracking conditions) [92–96].

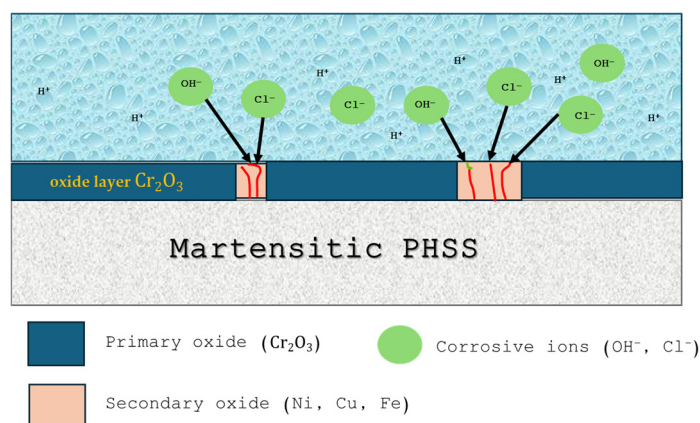


Figure 9. Schema of preference attacks in secondary oxides created during the passivation process. The secondary oxides are unstable.

The literature highlights that stainless steels develop a protective passive film enriched with oxides and hydroxides, distinct from films formed in natural conditions. Chemical passivation treatments typically remove surface contaminants, producing a cleaner and more protective passive film on stainless steel surfaces [97,98].

Using different techniques to characterize EN signals is important, and several authors have demonstrated that the statistical approach indicates that corrosion classification is largely inconsistent. This is attributed to LI variability; researchers like Eden and Mansfeld have pointed out the constraints of statistical evaluation, noting that Eden originally introduced LI years earlier to define corrosion types. Consequently, LI should be applied at the discretion of corrosion identification. Additionally, the signal examined using statistical methods must avoid a DC component to minimize standard deviation and yield a more precise outcome [99–101]. For that reason, in this research, recurrence plots were employed, and in this way, the results obtained by LI, kurtosis, and skewness were validated. It is important to mention that fact. The results obtained by recurrence plots helped to determine that if a well-localized process occurs on the surface, some samples will be passivated again. Conventional statistical methods cannot obtain that interpretation.

4. Conclusions

The present research investigates the passive state of passivated martensitic precipitation-hardening stainless steel in citric and nitric acid baths at 25 and 50 °C for 120 min and immersed in 1 wt.% H₂SO₄ and 5 wt.% NaCl solutions; considering the current results of experiments, the following can be concluded:

- The electrochemical noise results indicated that the martensitic precipitation-hardening stainless steel samples exposed to H₂SO₄ presented uniform pitting corrosion attacks.
- The samples exposed to NaCl presented pitting corrosion attacks. It is due to the susceptibility of PHSS to pitting generated by Cl[−] ions in preference zones due to the presence of two phases.
- The passivation of martensitic PHSS samples increased the corrosion resistance; however, the susceptibility to localized corrosion increased for passivated samples.
- Localized attacks occurred due to secondary oxide formation that facilitated surface differences, attacking in preference zones.
- Surface morphologies obtained by SEM indicate that the passivated martensitic precipitation-hardening stainless steel samples exhibit pitting corrosion, which is more intense when the steels are exposed to NaCl solution due to the aggressivity of Cl[−] ion.
- The best performance of passivation in nitric acid at 50 °C relates to the exothermic properties of the solution.
- The citric acid passivation process on stainless steels could be an environmentally friendly alternative to the frequently used nitric acid passivation process; however, it is necessary to increase research. The corrosion resistance increases, but the efficiency in comparison to nitric acid is lower.

Author Contributions: Conceptualization, C.G.-T., F.A.-C. and M.V.-T.; methodology, C.G.-T., M.V.-T., M.A.B.-Z., C.T.M.-R., J.O.-C., L.D.L.-L., J.M.J.-M., E.M.-B., D.N.-M. and V.A.-C.; formal analysis, C.G.-T., F.A.-C., M.A.B.-Z., C.T.M.-R., L.D.L.-L., E.M.-B., D.N.-M., G.S.-H. and V.A.-C.; data curation, C.G.-T., F.A.-C., C.T.M.-R., J.O.-C., D.N.-M., G.S.-H. and V.A.-C.; writing—review and editing, C.G.-T., F.A.-C. and J.M.J.-M.; investigation, G.S.-H. All authors have read and agreed to the published version of the manuscript.

Funding: This research received no external funding.

Data Availability Statement: The original contributions presented in this study are included in the article. Further inquiries can be directed to the corresponding authors.

Acknowledgments: The authors wish to thank the Academic Body UANL—CA-316 “Deterioration and integrity of composite materials” and Universidad Autónoma de Nuevo León (UANL) for the facilities provided for this investigation.

Conflicts of Interest: The authors declare no conflicts of interest.

References

1. Mouritz, P.A. *Introduction to Aerospace Materials*; Woodhead Publishing: Cambridge, UK, 2012.
2. Villegas-Tovar, J.; Gaona-Tiburcio, C.; Lara-Banda, M.; Maldonado-Bandala, E.; Baltazar-Zamora, M.A.; Cabral-Miramontes, J.; Nieves-Mendoza, D.; Olguin-Coca, J.; Estupiñán-Lopez, F.; Almeraya-Calderón, F. Electrochemical Corrosion Behavior of Passivated Precipitation Hardening Stainless Steels for Aerospace Applications. *Metals* **2023**, *13*, 835. [\[CrossRef\]](#)
3. Gialanella, S.; Malandrucolo, A. Aerospace Alloys. In *Topics in Mining, Metallurgy and Materials Engineering*; Bergmann, C.P., Ed.; Springer: Cham, Switzerland, 2020; ISSN 2364-3307. [\[CrossRef\]](#)
4. Samaniego-Gámez, O.; Almeraya-Calderón, F.; Chacón-Nava, J.; Maldonado-Bandala, E.; Nieves-Mendoza, D.; Flores-De los Rios, J.P.; Jáquez-Muñoz, J.M.; Delgado, A.D.; Gaona-Tiburcio, C. Corrosion Behavior of Passivated CUSTOM450 and AM350 Stainless Steels For Aeronautical Applications. *Metals* **2022**, *12*, 666. [\[CrossRef\]](#)
5. Cobb, H.M. *The History of Stainless Steel*; ASM International: Materials Park, OH, USA, 2010.
6. Lopes, J.C. Material selection for aeronautical structural application. *Sci. Technol. Adv. Mat.* **2008**, *20*, 78–82.
7. Farrar, J. *The Alloy Tree—A Guide to Low-Alloy Steels, Stainless Steels and Nickel-Base Alloys*; Woodhead Publishing Limited and CRC Press: Sawston, UK, 2004.
8. Almeraya-Calderón, F.; Samaniego-Gámez, O.; Maldonado-Bandala, E.; Nieves-Mendoza, D.; Olguin-Coca, J.; Jáquez-Muñoz, J.M.; Cabral-Miramontes, J.; Flores-De los Rios, J.P.; Bautista-Margulis, R.G.; Gaona-Tiburcio, C. Corrosion Behavior of Passivated Martensitic and Semi-Austenitic Precipitation Hardening Stainless Steel. *Metals* **2022**, *12*, 1033. [\[CrossRef\]](#)
9. ASM International. Introduction to Stainless Steel. In *Alloy Digest Sourcebook—Stainless Steel*, 3rd ed.; David, J.R., Davis & Associates, Eds.; ASM International: Materials Park, OH, USA, 2000; pp. 2–3.
10. Martínez-Villafañe, A.; Almeraya-Calderón, M.F.; Gaona-Tiburcio, C.; Gonzalez-Rodriguez, J.G.; Porcayo-Calderón, J. High-Temperature Degradation and Protection of Ferritic and Austenitic Steels in Steam Generators. *J. Mater. Eng. Perform.* **1998**, *7*, 108–113. [\[CrossRef\]](#)
11. Yu, Y.; Shironita, S.; Souma, K.; Umeda, M. Effect of chromium content on the corrosion resistance of ferritic stainless steels in sulfuric acid solution. *Heliyon* **2018**, *4*, e00958. [\[CrossRef\]](#)
12. Benavides, S. *Corrosion Control in the Aerospace Industry*; Woodhead Publishing: Cambridge, UK, 2009.
13. Lewis, P.; Kolody, M. Alternative to Nitric Acid Passivation of Stainless Steel Alloys. In *Technology Evaluation for Environmental Risk Mitigation Compendium, Proceedings of the NASA Technology Evaluation for Environmental Risk Mitigation Principal Center (TEERM)*; Department of Defense (DoD) and NASA, Kennedy Space Center: Merritt Island, FL, USA, 13 January 2008.
14. Gaona-Tiburcio, C.; Samaniego-Gámez, O.; Jáquez-Muñoz, J.M.; Baltazar-Zamora, M.A.; Landa-Ruiz, L.; Lira-Martínez, A.; los Rios, J.P.F.-D.; Cabral-Miramontes, J.; Estupiñán-López, F.; Almeraya-Calderon, F. Frequency-Time Domain Analysis of Electrochemical Noise of Passivated AM350 Stainless Steel for Aeronautical Applications. *Int. J. Electrochem. Sci.* **2022**, *17*, 220950. [\[CrossRef\]](#)
15. ASTM A967-17; Standard Specification for Chemical Passivation Treatments for Stainless Steel Parts. ASTM International: West Conshohocken, PA, USA, 1999.
16. Outokumpu. *Handbook of Stainless Steel*; Outokumpu Oyj: Helsinki, Finland, 2017.
17. Lin, C.K.; Tsai, W.J. Corrosion fatigue behaviour of a 15Cr-6Ni precipitation-hardening stainless steel in different tempers. *Fatigue Fract. Eng. Mater. Struct.* **2000**, *23*, 489–497. [\[CrossRef\]](#)
18. Mollapour, Y.; Poursaeidi, E. Experimental and numerical analysis of Pitting Corrosion in CUSTOM 450 Stainless Steel. *Eng. Fail. Anal.* **2021**, *128*, 105589. [\[CrossRef\]](#)
19. Lin, C.K.; Chu, C.C. Mean stress effects on low-cycle fatigue for a precipitation-hardening martensitic stainless steel in different tempers. *Fatigue Fract. Eng. Mater. Struct.* **2000**, *23*, 545–553. [\[CrossRef\]](#)
20. Almeraya-Calderon, F.; Villegas-Tovar, M.; Maldonado-Bandala, E.; Lara-Banda, M.; Baltazar-Zamora, M.A.; Santiago-Hurtado, G.; Nieves-Mendoza, D.; Lopez-Leon, L.D.; Jaquez-Muñoz, J.M.; Estupiñán-López, F.; et al. Use of Electrochemical Noise for the Study of Corrosion by Passivated CUSTOM 450 and AM 350 Stainless Steels. *Metals* **2024**, *14*, 341. [\[CrossRef\]](#)
21. Yasensky, D.; Reali, J.; Larson, C.; Carl, C. Citric acid passivation of stainless steel. In Proceedings of the Aircraft Airworthiness and Sustainment Conference, San Diego, CA, USA, 18–21 April 2009.

22. Yu, K.; Feng, S.; Ding, C.; Gu, M.; Yu, P.; Huang, M. A Sequential Dual-Passivation Strategy for Designing Stainless Steel Used above Water Oxidation. *Mater. Today* **2023**, *70*, 8–16. [\[CrossRef\]](#)
23. Oh, S.; Kim, D.; Kim, K.; Kim, D.I.; Chung, W.; Shin, B.H. The Effect of Surface Roughness on Re-Passivation and Pitting Corrosion of Super Duplex Stainless Steel UNS S 32760. *Int. J. Electrochem. Sci.* **2023**, *18*, 100351. [\[CrossRef\]](#)
24. Shen, Z. The Influence of Cr and Mo on the Formation of the Passivation Film on the Surface of Ferritic Stainless Steel. *Mater. Today Commun.* **2024**, *38*, 108221. [\[CrossRef\]](#)
25. Yu, K.P.; Chen, X.L.; Ye, K.Q.; Huang, M.X. Counterintuitive Passivation Role of Manganese in Stainless Steel under High Potential in Neutral NaCl Solution. *Corros. Sci.* **2025**, *246*, 112756. [\[CrossRef\]](#)
26. Vukkum, V.B.; Christudasjustus, J.; Darwish, A.A.; Storck, S.M.; Gupta, R.K. Enhanced Corrosion Resistance of Additively Manufactured Stainless Steel by Modification of Feedstock. *npj Mater. Degrad.* **2022**, *6*, 2. [\[CrossRef\]](#)
27. Shin, B.H.; Park, J.; Jeon, J.; Heo, S.b.o.; Chung, W. Effect of Cooling Rate after Heat Treatment on Pitting Corrosion of Super Duplex Stainless Steel UNS S 32750. *Anti-Corros. Methods Mater.* **2018**, *65*, 492–498. [\[CrossRef\]](#)
28. Köse, C. Effect of Heat Input and Post Weld Heat Treatment on the Texture, Microstructure and Mechanical Properties of Laser Beam Welded AISI 317L Austenitic Stainless Steel. *Mater. Sci. Eng. A* **2022**, *855*, 143966. [\[CrossRef\]](#)
29. Man, C.; Dong, C.; Cui, Z.; Xiao, K.; Yu, Q.; Li, X. A comparative study of primary and secondary passive films formed on AM355 stainless steel in 0.1 M NaOH. *Appl. Surf. Sci.* **2018**, *427*, 763–773. [\[CrossRef\]](#)
30. Bojinov, M.; Betova, I.; Fabricius, G.; Laitinen, T.; Saario, T. The stability of the passive state of iron–chromium alloys in sulphuric acid solution. *Corros. Sci.* **1999**, *41*, 1557–1584. [\[CrossRef\]](#)
31. Núñez-Jaquez, R.E.; Buelna-Rodríguez, J.E.; Barrios-Durstewitz, C.P.; Gaona-Tiburcio, C.; Almeraya-Calderón, F. Corrosion of modified concrete with sugar cane bagasse ash. *Int. J. Corros.* **2012**, *2012*, 451864. [\[CrossRef\]](#)
32. Almeraya-Calderón, F.; Villegas-Tovar, M.; Maldonado-Bandala, E.; Lara-Banda, M.; Baltazar-Zamora, M.A.; Landa-Ruiz, L.; Nieves-Mendoza, D.; Jaquez-Muñoz, J.M.; Estupiñán-Lopez, F.; Cabral-Miramontes, J.; et al. Localized Corrosion of CUSTOM 450 and AM 350 Stainless Steels in H₂SO₄ and NaCl Solutions. *Materials* **2025**, *18*, 988. [\[CrossRef\]](#)
33. Alireza, R.; Abdolreza, F.; Avni, B.; Alireza, S.; Mikhail, A.V.; Valbonë, M.; Zhong, X.; Samira, Y.; Richard, D. Novel sucrose derivative as a thermally stable inhibitor for mild steel corrosion in 15% HCl medium: An experimental and computational study. *Chem. Eng. J.* **2022**, *446*, 136938. [\[CrossRef\]](#)
34. Suresh, G.U.; Kamachi, M.S. Electrochemical Noise Analysis of Pitting Corrosion of Type 304L Stainless Steel. *Corrosion* **2014**, *70*, 283–293. [\[CrossRef\]](#)
35. Lara-Banda, M.; Gaona-Tiburcio, C.; Zambrano-Robledo, P.; Delgado-E, M.; Cabral-Miramontes, J.; Nieves-Mendoza, D.; Maldonado-Bandala, E.; Estupiñán-Lopez, F.; Chacón-Nava, J.; Almeraya-Calderón, F. Alternative to Nitric Acid Passivation of 15-5 and 17-4PH Stainless Steel Using Electrochemical Techniques. *Materials* **2020**, *13*, 2836. [\[CrossRef\]](#)
36. Bragaglia, M.; Cherubini, V.; Cacciotti, I.; Rinaldi, M.; Mori, S.; Soltani, P.; Nanni, F.; Kaciulis, S.; Montesperelli, G. Citric Acid Aerospace Stainless Steel Passivation: A Green Approach. In Proceedings of the CEAS Aerospace Europe Conference 2015, Delft, The Netherlands, 7–11 September 2015.
37. Marcelin, S.; Pébèrea, N.; Régnier, S. Electrochemical characterisation of a martensitic stainless steel in a neutral chloride solution. *Electrochim. Acta* **2013**, *87*, 32–40. [\[CrossRef\]](#)
38. El-Taib Heakal, F.; Ghoneim, A.; Fekry, A. Stability of spontaneous passive films on high strength Mo-containing stainless steels in aqueous solutions. *J. Appl. Electrochem.* **2007**, *37*, 405–413. [\[CrossRef\]](#)
39. El-Taib Heakal, F.; Ameer, M.A.; El-Aziz, A.M.; Fekry, A.M. Electrochemical behavior of Mo-containing austenitic stainless steel in buffer solutions. *Mater. Sci. Eng. Technol.* **2004**, *35*, 407–413. [\[CrossRef\]](#)
40. Fakić, B.; Čubela, D. Review of the Development of Research in the Design of Semi Austenitic Stainless Steel 17-7PH. In Proceedings of the 17th International Research/Expert Conference “Trends in the Development of Machinery and Associated Technology” TMT 2013, Istanbul, Turkey, 10–11 September 2013; pp. 113–116.
41. Warren, J.; Wei, D.Y. The low cycle fatigue behavior of the controlled transformation stainless steel alloy AM355 at 121, 204 and 315 °C. *Mater. Sci. Eng. A* **2008**, *475*, 148–156. [\[CrossRef\]](#)
42. Yang, S.; Ma, J.; Chen, C.; Zhang, C.; Ren, J.; Jiang, Z.; Fan, G.; Han, P. Effects of B and Ce Grain Boundary Segregation on Precipitates in Super Austenitic Stainless Steel. *Metals* **2023**, *13*, 326. [\[CrossRef\]](#)
43. Wang, T.; Wang, J.; Bai, J.; Wang, S.; Chen, C.; Han, P. Effect of boron on dissolution and repairing behavior of passive film on S31254 super-austenitic stainless steel immersed in H₂SO₄ solution. *J. Iron Steel Res. Int.* **2022**, *29*, 1012–1025. [\[CrossRef\]](#)
44. Shaikh, H.; George, G.; Khatak, H.S. Failure analysis of an AM 350 steel bellows. *Eng. Fail. Anal.* **2001**, *8*, 571–576. [\[CrossRef\]](#)
45. Jaquez-Muñoz, J.; Gaona-Tiburcio, C.; Lira-Martinez, A.; Zambrano-Robledo, P.; Maldonado-Bandala, E.; Samaniego-Gamez, O.; Nieves-Mendoza, D.; Olguin-Coca, J.; Estupiñán-Lopez, F.; Almeraya-Calderon, F. Susceptibility to pitting corrosion of Ti-CP2, Ti-6Al-2Sn-4Zr-2Mo, and Ti-6Al-4V alloys for aeronautical applications. *Metals* **2021**, *11*, 1002. [\[CrossRef\]](#)

46. Kumar, T.S.; Ramanujam, R.; Vignesh, M.; Rohith, D.; Manoj, V.; Sankar, P.H. Comparative machining studies on custom 450 alloy with TiCN, TiAlN coated and uncoated carbide tools using Taguchi-Fuzzy logic approach. *Mater. Res. Express* **2019**, *6*, 066411. [CrossRef]
47. Jáquez-Muñoz, J.M.; Gaona-Tiburcio, C.; Méndez-Ramírez, C.T.; Baltazar-Zamora, M.Á.; Estupinán-López, F.; Bautista-Margulis, R.G.; Cuevas-Rodríguez, J.; Flores-De los Rios, J.P.; Almeraya-Calderón, F. Corrosion of Titanium Alloys Anodized Using Electrochemical Techniques. *Metals* **2023**, *13*, 476. [CrossRef]
48. Custom 450® Stainless Steel. Available online: <https://www.ulbrich.com/uploads/data-sheets/Custom-450-Stainless-Steel-Wire-UNS-S45000.pdf> (accessed on 30 March 2025).
49. ASTM G199-90; Standard Guide for Electrochemical Noise Measurement. ASTM International: West Conshohocken, PA, USA, 1995.
50. ASTM E3-95; Standard Practice for Preparation of Metallographic Specimens. ASTM International: West Conshohocken, PA, USA, 1995.
51. Gallego-Juárez, J.A.; Graff, K.F. *Power Ultrasonics-Applications of High-Intensity Ultrasound*; Woodhead Publishing: Sawston, UK, 2015.
52. The British Stainless Steel Association. 2022. Available online: https://bssa.org.uk/bssa_articles/calculation-of-pren/ (accessed on 2 February 2025).
53. Lara-Banda, M.; Ortiz, D.; Gaoan-Tiburcio, C.; Zambrano, P.; Cabral-Miramontes, J.C.; Almeraya- Calderon, F. Citric Acid Passivation of 15-5PH and 17-4PH Stainless Steel Used in the Aeronautical Industry. In *International Materials Research Congress*; Springer: Cham, Switzerland, 2016; pp. 95–104.
54. ASTM A380-17; Standard Practice for Cleaning, Descaling and Passivation of Stainless-Steel Parts, Equipment, and Systems. ASTM International: West Conshohocken, PA, USA, 1999.
55. SAE AMS 2700F; Passivation of Corrosion Resistant Steels. Aerospace Material Specification. SAE International: Warrendale, PA, USA, 2018.
56. ASTM G199-09; Standard Guide for Electrochemical Noise Measurement. ASTM International: West Conshohocken, PA, USA, 2020.
57. Cottis, R. Interpretation of Electrochemical Noise Data. *Corrosion* **2001**, *57*, 265–285. [CrossRef]
58. Martinez, B.; Tiburcio, C.G.; Bastidas, D.; Lara-Banda, M.; Samaniego, O.; Calderon, F.A. Electrochemical Evaluation of 15-5PH Stainless Steel Passivated in Citric Acid. *ECS Trans.* **2022**, *106*, 223. [CrossRef]
59. Silverman, D.C. Tutorial on Cyclic Potentiodynamic Polarization Technique. In Proceedings of the CORROSION 98, San Diego, CA, USA, 22–27 March 1998.
60. Silverman, D.C. Practical Corrosion Prediction Using Electrochemical Techniques. In *Uhlig's Corrosion Handbook*, 3rd ed.; Wiley: Hoboken, NJ, USA, 2011; pp. 1129–1166. [CrossRef]
61. STP1277-EB; Electrochemical Noise Measurement for Corrosion Applications. ASTM International: West Conshohocken, PA, USA, 2015.
62. Sanchez-Amaya, J.M.; Cottis, R.A.; Botana, F.J. Shot Noise and Statistical Parameters for the Estimation of Corrosion Mechanisms. *Corros. Sci.* **2005**, *47*, 3280–3299. [CrossRef]
63. Turgoose, S.; Cottis, R.A. *Electrochemical Impedance and Noise*; NACE International: Houston, TX, USA, 2009; ISBN 1575900939.
64. Galvan-Martinez, R.; Orozco-Cruz, R.; Torres-Sanchez, R.; Martinez, E.A. Corrosion Study of the X52 Steel Immersed in Seawater with a Corrosion Inhibitor Using a Rotating Cylinder Electrode. *Mater. Corros.* **2010**, *61*, 872–876. [CrossRef]
65. Bertocci, U.; Huet, F. Noise Analysis Applied to Electrochemical Systems. *Corrosion* **1995**, *51*, 131–144. [CrossRef]
66. Bertocci, U.; Kruger, J. Studies of Passive Film Breakdown by Detection and Analysis of Electrochemical Noise. *Surf. Sci.* **1980**, *101*, 608–618. [CrossRef]
67. Al-Zanki, I.A.; Gill, J.S.; Dawson, J.L. Electrochemical Noise Measurements on Mild Steel in 0.5 M Sulphuric Acid. *Mater. Sci. Forum* **1986**, *8*, 463–476. [CrossRef]
68. Eden, D.A.; Rothwell, A.N. *Electrochemical Noise Data: Analysis, Interpretation and Presentation*; NACE International: Houston, TX, USA, 1992; pp. 1–12.
69. Bertocci, U.; Gabrielli, C.; Huet, F.; Keddam, M.; Rousseau, P. Noise Resistance Applied to Corrosion Measurements: II. Experimental Tests. *J. Electrochem. Soc.* **1997**, *144*, 37–43. [CrossRef]
70. Eden, D.A.; John, D.G.; Dawson, J.L. International Patent WO 87/07022, 19 November 1987.
71. Mansfeld, F.; Sun, Z.; Hsu, C.H.; Nagiub, A. Concerning Trend Removal in Electrochemical Noise Measurements. *Corros. Sci.* **2001**, *43*, 341–352. [CrossRef]
72. Lee, C.C.; Mansfeld, F. Analysis of Electrochemical Noise Data for a Passive System in the Frequency Domain. *Corros. Sci.* **1998**, *40*, 959–962. [CrossRef]
73. Homborg, A.M.; Tinga, T.; Van Westing, E.P.M.; Zhang, X.; Ferrari, G.M.; De Wit, J.H.W.; Mol, J.M.C. A Critical Appraisal of the Interpretation of Electrochemical Noise for Corrosion Studies. *Corrosion* **2014**, *70*, 971–987. [CrossRef]

74. Chen, A.; Cao, F.; Liao, X.; Liu, W.; Zheng, L.; Zhang, J.; Cao, C. Study of Pitting Corrosion on Mild Steel during Wet–Dry Cycles by Electrochemical Noise Analysis Based on Chaos Theory. *Corros. Sci.* **2013**, *66*, 183–195. [\[CrossRef\]](#)
75. Mansfeld, F.; Sun, Z. Technical Note: Localization Index Obtained from Electrochemical Noise Analysis. *Corrosion* **1999**, *55*, 915–918. [\[CrossRef\]](#)
76. Reid, S.A.; Eden, D.A. Assessment of Corrosion. U.S. Patent US9264824B1, 24 July 2001.
77. Eden, D.A. Electrochemical Noise—The First Two Octaves. In *Proceedings of the NACE—International Corrosion Conference Series*; OnePetro: Richardson, TX, USA, 1998.
78. Dawson, D.L. Electrochemical Noise Measurement: The definitive In-Situ Technique for Corrosion Applications? In *Electrochemical Noise Measurement for Corrosion Applications STP 1277*; Kearns, J.R., Scully, J.R., Roberge, P.R., Reirchert, D.L., Dawson, L., Eds.; ASTM International, Materials Park: Russell, OH, USA, 1996; pp. 3–39.
79. Almeraya-Calderón, F.; Jáquez-Muñoz, J.M.; Maldonado-Bandala, E.; Cabral-Miramontes, J.; Nieves-Mendoza, D.; Olgui-Coca, J.; Lopez-Leon, L.D.; Estupiñán-López, F.; Lira-Martínez, A.; Gaona Tiburcio, C. Corrosion Resistance of Titanium Alloys Anodized in Alkaline Solutions. *Metals* **2023**, *13*, 1510. [\[CrossRef\]](#)
80. Ye, Z.; Guan, L.; Li, Y.; Zhong, J.; Liao, L.; Xia, D.; Huang, J. Understanding the Galvanic Corrosion of Cu-Ni Alloy/2205 DSS Couple Using Electrochemical Noise and Microelectrochemical Studies. *Corros. Sci.* **2023**, *224*, 111512. [\[CrossRef\]](#)
81. Bojinov, M.; Fabricius, G.; Kinnunen, P.; Laitinen, T.; Mäkelä, K.; Saario, T.; Sundholm, G. The mechanism of transpassive dissolution of Ni–Cr alloys in sulphate solutions. *Electrochim. Acta* **2000**, *45*, 2791–2802. [\[CrossRef\]](#)
82. Huang, J.; Wu, X.; Han, E.H. Electrochemical properties and growth mechanism of passive films on Alloy 690 in high-temperature alkaline environments. *Corros. Sci.* **2010**, *52*, 3444–3452. [\[CrossRef\]](#)
83. Calinski, C.; Strehblow, H.H. ISS depth profiles of the passive layer on Fe/Cr alloys. *J. Electrochem. Soc.* **1989**, *36*, 1328–1331. [\[CrossRef\]](#)
84. Xia, D.-H.; Song, S.; Behnamian, Y.; Hu, W.; Cheng, Y.F.; Luo, J.-L.; Huet, F. Review—Electrochemical Noise Applied in Corrosion Science: Theoretical and Mathematical Models towards Quantitative Analysis. *J. Electrochem. Soc.* **2020**, *167*, 081507. [\[CrossRef\]](#)
85. Fattah-alhosseini, A.; Taheri Shoja, S.; Heydari Zebardast, B.; Mohamadian Samim, P. An Electrochemical Impedance Spectroscopic Study of the Passive State on AISI 304 Stainless Steel. *Int. J. Electrochem.* **2011**, *2011*, 152143. [\[CrossRef\]](#)
86. Castro, B.E.; Vilche, R.J. Investigation of passive layers on iron and iron-chromium alloys by electrochemical impedance spectroscopy. *Electrochim. Acta* **1993**, *38*, 1567–1572. [\[CrossRef\]](#)
87. Luo, Z.G.; Zhang, Y.; Wang, H.; Wan, S.; Song, L.F.; Liao, B.K.; Guo, X.P. Modified nano-lignin as a novel biomass-derived corrosion inhibitor for enhanced corrosion resistance of carbon steel. *Corros. Sci.* **2024**, *227*, 111705. [\[CrossRef\]](#)
88. Cuevas-Arteaga, C.; Porcayo-Calderón, J. Electrochemical noise analysis in the frequency domain and determination of corrosion rates for SS-304 stainless steel. *Mater. Sci. Eng. A* **2006**, *435–436*, 439–446. [\[CrossRef\]](#)
89. Martínez-Aparicio, B.; Martínez-Bastidas, D.; Gaona-Tiburcio, C.; Martín, U.; Cabral-Miramontes, J.; Almeraya-Calderón, F. Localized corrosion of 15–5 PH and 17–4 PH stainless steel in NaCl solution. *J. Solid State Electrochem.* **2023**, *11*, 2993–3001. [\[CrossRef\]](#)
90. Liao, X.; Du, L.; Pei, J.; Hu, Y.; Liu, J. Citric Acid Enhances the Ignition and Combustion Performance of Aluminum: Coating and Etching. *Colloids Surfaces A Physicochem. Eng. Asp.* **2024**, *689*, 133628. [\[CrossRef\]](#)
91. Garcia-Ochoa, E.; Maldonado, P.; Corvo, F. Non-linear Dynamics of Potassium Iodide Adsorption on the Interface of Carbon Steel in Acidic Medium. *Mater. Corros.* **2020**, *71*, 1152–1159. [\[CrossRef\]](#)
92. Marwan, N.; Webber, C.L.; Macau, E.E.N.; Viana, R.L. Introduction to Focus Issue: Recurrence Quantification Analysis for Understanding Complex Systems. *Chaos* **2018**, *28*, 85601. [\[CrossRef\]](#)
93. Valavanis, D.; Spanoudaki, D.; Gkili, C.; Sazou, D. Using Recurrence Plots for the Analysis of the Non-linear Dynamical Response of Iron Passivation-Corrosion Processes. *Chaos* **2018**, *28*, 085708. [\[CrossRef\]](#)
94. Martínez-Ramos, C.; Olgui-Coca, J.; Lopez-Leon, L.D.; Gaona-Tiburcio, C.; Lara-Banda, M.; Maldonado-Bandala, E.; Castañeda-Robles, I.; Jaquez-Muñoz, J.M.; Cabral-Miramontes, J.; Nieves-Mendoza, D.; et al. Electrochemical Noise Analysis Using Experimental Chaos Theory, Power Spectral Density and Hilbert–Huang Transform in Anodized Aluminum Alloys in Tartaric–Phosphoric–Sulfuric Acid Solutions. *Metals* **2023**, *13*, 1850. [\[CrossRef\]](#)
95. Grünleitner, T.; Henning, A.; Bissolo, M.; Zengerle, M.; Gregoratti, L.; Amati, M.; Zeller, P.; Eichhorn, J.; Stier, A.V.; Holleitner, A.W.; et al. Real-Time Investigation of Sulfur Vacancy Generation and Passivation in Monolayer Molybdenum Disulfide via in Situ X-Ray Photoelectron Spectromicroscopy. *ACS Nano* **2022**, *16*, 20364–20375. [\[CrossRef\]](#)
96. Wang, Z.; Di-Franco, F.; Seyeux, A.; Zanna, S.; Maurice, V.; Marcus, P. Passivation-Induced Physicochemical Alterations of the Native Surface Oxide Film on 316L Austenitic Stainless Steel. *J. Electrochem. Soc.* **2019**, *166*, C3376–C3388. [\[CrossRef\]](#)
97. Gao, Y.; Chong, K.; Qiao, L.; Li, Y.; Liu, C.; Guo, F.; Wu, D.; Zou, Y. Synthesis and Corrosion Behavior of Mo₁₅Nb₂₀Ta₁₀Ti₃₅V₂₀ Refractory High Entropy Alloy. *Mater. Des.* **2023**, *228*, 111820. [\[CrossRef\]](#)
98. Zhao, Z.; Peng, S.; Ma, C.; Yu, C.; Wu, D. Redox Behavior of Secondary Solid Iron Species and the Corresponding Effects on Hydroxyl Radical Generation during the Pyrite Oxidation Process. *Environ. Sci. Technol.* **2022**, *56*, 12635–12644. [\[CrossRef\]](#)

99. Liu, G.; Tong, H.; Li, Y.; Tan, Q.; Zhu, Y. Passivation Behavior of S136H Steel in Neutral Electrolytes Composed of NaClO₃ and NaNO₃ and Its Influence on Micro Electrochemical Machining Performance. *Mater. Today Commun.* **2021**, *29*, 102762. [[CrossRef](#)]
100. Wu, B.R.; Yao, J.T.; Dong, H.; Chen, Z.L.; Liu, X.G. Enhancing the Corrosion Resistance of Passivation Films via the Synergistic Effects of Graphene Oxide and Epoxy Resin. *Coatings* **2025**, *15*, 444. [[CrossRef](#)]
101. Botona Pedemonte, F.J.; Aballe Villero, A.; Marcos Bárcena, M. *Ruido Electroquímico. Métodos de Análisis*; Septem Ediciones, S.L.: Oviedo, Spain, 2002; ISBN 84-95687-33-X.

Disclaimer/Publisher's Note: The statements, opinions and data contained in all publications are solely those of the individual author(s) and contributor(s) and not of MDPI and/or the editor(s). MDPI and/or the editor(s) disclaim responsibility for any injury to people or property resulting from any ideas, methods, instructions or products referred to in the content.